magnetism

MDPI

Article

Tuning of the Magnetocaloric Properties of Mn_5Ge_3 Compound by Chemical Modification

Karol Synoradzki [1,*], Krzysztof Urban [1,2], Przemysław Skokowski [1], Hubert Głowiński [1] and Tomasz Toliński [1]

[1] Institute of Molecular Physics, Polish Academy of Sciences, M. Smoluchowskiego 17, 60-179 Poznań, Poland; krzysztof.urban.93@gmail.com (K.U.); przemyslaw.skokowski@ifmpan.poznan.pl (P.S.); hubert.glowinski@ifmpan.poznan.pl (H.G.); tomtol@ifmpan.poznan.pl (T.T.)

[2] Faculty of Material Engineering and Technical Physic, Poznan University of Technology, Piotrowo 3, 60-965 Poznań, Poland

* Correspondence: karol.synoradzki@ifmpan.poznan.pl; Tel.: +48-618-695-282

Abstract: The rare earth-free Mn_5Ge_3 compound shows magnetocaloric properties similar to those of pure Gd; therefore, it is a good candidate for magnetic refrigeration technology. In this work, we investigate the influence of chemical substitution on the crystal structure and the magnetic, thermodynamic, and magnetocaloric properties of a polycrystalline Mn_5Ge_3 compound prepared by induction melting. For this purpose, we replaced 5% of the Mn with Cr or Co and 5% of the Ge with B or Al. The additional chemical elements were shown not to change the crystal structure of the parent compound (space group $P6_3/mcm$, No. 193). In the case of the magnetic properties, all samples remained ferromagnetic with the ordering temperature (T_C) lower than for the original compound (T_C = 295(1) K). The exception was the sample with B, where we observed an increase in T_C by 3 K. The maximum value of the magnetic entropy change, $|\Delta S_m|^{MAX}$ (for a magnetic field change of 5 T), decreased from 7.1(1) for Mn_5Ge_3 to 6.2(1), 6.8(1), 4.8(1), and 5.8(1) J kg^{-1} K^{-1} for the alloys with B, Al, Cr, and Co, respectively. The adiabatic temperature change (ΔT_{ad}) (for a magnetic field change of 1 T) was determined from the specific heat measurements and was equal to 1.1(1), 1.2(1), 1.2(1), 0.8(1), and 0.8(1) K for Mn_5Ge_3, $Mn_5Ge_{2.85}B_{0.15}$, $Mn_5Ge_{2.85}Al_{0.15}$, $Mn_{4.75}Cr_{0.25}Ge_3$, and $Mn_{4.75}Co_{0.25}Ge_3$, respectively. The obtained data were compared with those from the literature. It was found that the substitution allowed for tuning of the ordering temperature in a wide temperature range. At the same time, the reduction in the magnetocaloric parameters' values was relatively small. Therefore, the produced Mn_5Ge_3-based alloys allow for the expansion of the operation temperature range of the parent compound as a magnetocaloric material.

Keywords: Mn_5Ge_3; magnetocaloric effect; refrigeration capacity; adiabatic temperature change; magnetic refrigeration

Citation: Synoradzki, K.; Urban, K.; Skokowski, P.; Głowiński, H.; Toliński, T. Tuning of the Magnetocaloric Properties of Mn_5Ge_3 Compound by Chemical Modification. *Magnetism* **2022**, 2, 56–73. https://doi.org/10.3390/magnetism2010005

Academic Editors: Tarek Bachagha and Joan-Josep Suñol

Received: 20 December 2021
Accepted: 28 January 2022
Published: 3 March 2022

1. Introduction

The magnetocaloric effect is a phenomenon that leads to a change in the temperature of a magnetic material under the influence of an external magnetic field [1], and it can be employed in various devices (e.g., refrigerators) operating over a wide temperature range [2]. It has been shown that household appliances based on this technology (e.g., refrigerators and air conditioners) can consume less electricity and be more environmentally friendly, as they do not work with greenhouse or ozone-depleting gases. New materials with suitable properties are necessary for the development of magnetic cooling technology [3–5]. The search for such materials has been going on continuously for many years. Materials that exhibit a large magnetocaloric effect around room temperature include Gd [6,7], $Gd_5(Si,Ge)_4$ [8,9], FeRh [10,11], $La(Fe,Si,X)_{13}H_x$ [12], $La(Fe,Si)_{13}$ [13], Ni–Mn–In Heusler alloys [14,15], Mn–Fe–P–As alloys [16], and MnAs alloys [17].

The same technology can be used to build coolers that operate at low temperatures, which can be used to liquefy helium, hydrogen, or natural gas [18]. Therefore, magnetocaloric materials capable of working in a wide temperature range are also being sought. The such hitherto known materials include many intermetallic alloys and compounds (e.g., Laves phases [19,20]), especially those containing rare earth elements [21–24].

Another subgroup of magnetocaloric materials with high potential are the compounds and alloys containing Mn [25–28]. This is because the value of MCE strongly depends on the value of the magnetic moment, which is particularly high for Mn and thus also for Mn-based materials. One of the most interesting compounds based on Mn is Mn_5Ge_3, which has attracted attention in many research fields for more than 50 years, e.g., in magnetic domain structure studies [29] or in spintronics as a possible efficient spin-injector due to the high spin-polarization of Mn_5Ge_3 and compatibility with Ge-based technology [30–35]. Mn_5Ge_3 is a promising magnetocaloric material because it is a soft ferromagnet showing second-order phase transition with a Curie temperature (T_C) near room temperature, a large magnetic entropy change of ΔS_m = 7–9 J kg^{-1} K^{-1} for a magnetic field change of 5 T [36–38], and an adiabatic temperature change of ΔT_{ad} = 1 K for a magnetic field change of 1 T [36]. This compound, owing to its physical properties, may be used in magnetic refrigerators [39,40]. The attractive properties of Mn_5Ge_3 initiated studies of, for example, off-stoichiometric $Mn_{5+x}Ge_{3-x}$ alloys [41] or systems modified chemically by introducing elements such as Co [42–45], Fe [42,44–47], or Ni [48] into the Mn position or by replacing Ge with Si [49,50], Ga [51], Sb [52], Al [53], Ag [54,55], or even Fe [56]. Moreover, simultaneous substitutions of Fe for Mn and Si for Ge have also been attempted [57,58]. The goal of all these modifications was to increase the application potential of Mn_5Ge_3. In addition, due to the high price of pure Ge (>1000 USD/kg), the cost of raw materials for an Mn_5Ge_3 compound is too high for commercial application in terms of magnetic refrigeration [5]. Therefore, partial replacement of Ge with cheaper elements may not only improve its magnetocaloric properties, but also reduce the cost.

In this work, we joined the trend of investigating the effect of chemical composition modification on the magnetocaloric properties of the Mn_5Ge_3 compound. For this purpose, we prepared samples with novel substitutions or with a level of modification not yet investigated. The alloys with the chemical composition $Mn_5Ge_{2.85}B_{0.15}$, $Mn_5Ge_{2.85}Al_{0.15}$, $Mn_{4.75}Cr_{0.25}Ge_3$, and $Mn_{4.75}Co_{0.25}Ge_3$ were examined from the point of view of their structural, magnetic, thermodynamic, and magnetocaloric properties. It was found that any changes in the stoichiometry of the starting material had a considerable effect on its properties. The most interesting results were obtained for the compound $Mn_5Ge_{2.85}B_{0.15}$.

Unlike previous studies in the literature where arc-melting was used for synthesis, here the induction melting process was used to obtain the materials studied.

2. Materials and Methods

Polycrystalline samples of $(Mn_{1-x}Me_x)_5(Ge_{1-y}Oe_y)_3$ (*Me* = Co, Cr; *Oe* = B, Al; x, y = 0.05) alloys were synthesized by induction melting of pure (i.e., Mn, 99.9%; Ge, 99.9999%; Co, 99.998%; Cr, 99.99%; B, 99.999%; Al, 99.999%) constituent elements in a water-cooled copper hearth under a high-purity argon atmosphere. Pellets of approximately 2 g each were remelted and flipped several (at least five) times to ensure homogeneity. No additional Mn was added to the initially calculated mass. However, Mn was remelted before adding it to the batch to improve its quality. The total mass loss for each sample was less than 0.1%. Afterwards, no further heat treatment was applied. The density of the samples was determined by the Archimedes method at room temperature. To measure the mass of the samples, a Radwag (Radom, Poland) XA 110.4Y.A electronic scale was used.

The phase purity of all the compounds was checked by Rietveld analysis of the X-ray diffraction (XRD) patterns collected at room temperature. A diffractometer with a Bragg–Brentano configuration equipped with a Cu-Kα radiation source was used. The structure refinement was carried out by employing the program FullProf (version 6.30) [59].

Scanning electron microscopy (SEM) images and the elemental compositions were obtained using an FEI Nova NanoSEM 650 with an energy-dispersive spectroscopy (EDS) attachment. An electron energy of 30 keV was used for imaging and excitation of the characteristic radiation of the elements. Analysis of the EDS data was performed with the license software delivered with the instrument using the P/B ZAF (standardless) method.

Magnetic field and temperature dependent magnetization data were collected using a Physical Property Measurement System (PPMS, Quantum Design, San Diego, CA, USA) equipped with a vibrating sample magnetometer (VSM). Measurements of magnetization as a function of temperature were made in two modes. First, the zero-field cooling (ZFC) mode was used, i.e., the sample was first cooled down to 2 K without magnetic field and then the measurement was performed during heating. Next, the field cooling (FC) mode was employed in which the sample was cooled in a constant non-zero magnetic field down to the lowest temperatures while the magnetization measurement was performed. Both measurements were made in the temperature range from 2 to 400 K.

Measurements of the specific heat in the temperature range from 260 to 380 K were made using the 2τ relaxation method with the heat capacity option of the PPMS. Samples of ~10 mg were attached to the platform with Apiezone H.

3. Results and Discussion

First, the structures of the obtained samples were determined. The room temperature XRD patterns for all studied $(Mn_{1-x}Me_x)_5(Ge_{1-y}Oe_y)_3$ alloys are presented in Figure 1. The Rietveld refinement of the powder XRD patterns of all the compounds showed a hexagonal crystal structure with a space group $P6_3/mcm$ (No. 193). In this structure, Mn atoms occupied two positions, 4*d* (1/3, 2/3, 0) and 6*g* (x_1, 0, 1/4), whereas Ge atoms occupied only the 6*g* (x_2, 0, 1/4) sites [60]. Exemplary results of the Rietveld analysis are shown in Figure 1a,b for selected samples (modified by B and Co substitution). The lattice parameters estimated for all of the compounds from the refinement are shown in Table 1. It was found that the lattice parameters values did not change significantly, and for the Co substitution, they were comparable with those from the literature [42,44,45]. In addition to the main diffraction peaks originating from the hexagonal structure, some small peaks (marked by the star symbol in Figure 1) assigned to minor unknown impurity phases can be observed for some of the samples.

As shown previously, the average size of the crystallites, *D*, can strongly influence the magnetic and magnetocaloric properties of different materials [36,61,62]. Therefore, for comparative studies, it is preferred to study materials with crystallites of similar size. *D* was calculated from the standard Scherrer formula: $D = 0.89\lambda/B\cos\theta_d$, where λ is the X-ray wavelength, *B* is the full width at half maximum of a peak, and θ_d is the Bragg angle [63]. The values of *D* for the $(Mn_{1-x}Me_x)_5(Ge_{1-y}Oe_y)_3$ alloys are listed in Table 1. It turns out that for our samples, the values of *D* were very similar and close to 50 nm.

Table 1. The estimated chemical composition, the lattice parameters (*a*, *c*) values, the unit-cell volume (*V*), the average crystallite size (*D*), and the theoretical (d_t) and experimental (*d*) densities for the $(Mn_{1-x}Me_x)_5(Ge_{1-y}Oe_y)_3$ alloys.

Alloy	Estimated Composition	*a* (Å)	*c* (Å)	*V* (Å^3)	*D* (nm)	d_t (g/cm^3)	*d* (g/cm^3)
Mn_5Ge_3	$Mn_{5.04(8)}Ge_{2.96(8)}$	7.203(2)	5.041(1)	226.5(1)	52(8)	7.243	7.04(6)
$Mn_5(Ge_{0.95}B_{0.05})_3$	$Mn_{5.08(8)}Ge_{2.81(8)}B_{0.11(8)}$	7.204(8)	5.041(6)	226.5(5)	48(3)	7.097	6.69(5)
$Mn_5(Ge_{0.95}Al_{0.05})_3$	$Mn_{5.04(8)}Ge_{2.83(8)}Al_{0.13(8)}$	7.209(3)	5.037(3)	226.7(2)	49(3)	7.238	6.95(2)
$(Mn_{0.95}Cr_{0.05})_5Ge_3$	$Mn_{4.88(8)}Cr_{0.22(8)}Ge_{2.90(8)}$	7.209(17)	5.042(12)	226.9(1)	45(5)	7.268	6.90(9)
$(Mn_{0.95}Co_{0.05})_5Ge_3$	$Mn_{4.76(8)}Co_{0.25(8)}Ge_{2.99(8)}$	7.197(15)	5.030(11)	225.6(1)	41(4)	7.284	6.92(4)

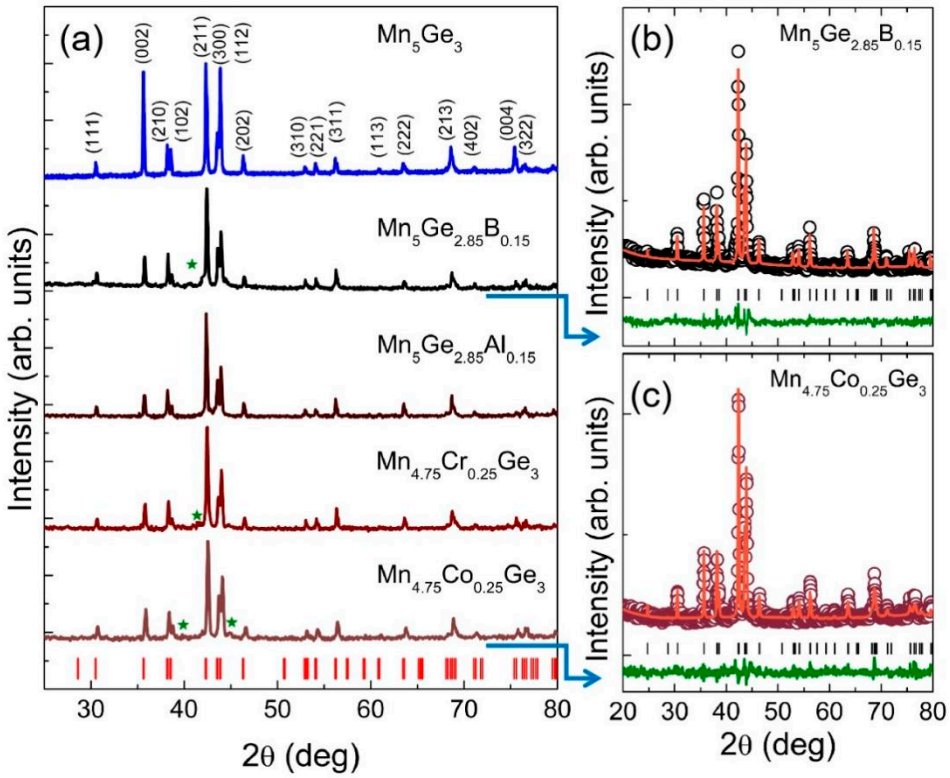

Figure 1. (**a**) XRD data obtained at room temperature for all of the studied $(Mn_{1-x}Me_x)_5(Ge_{1-y}Oe_y)_3$ alloys. Vertical ticks at the bottom indicate the Bragg maxima positions for Mn_5Ge_3 labeled with the Miller indices at the top. Stars mark the peaks due to the impurity phases. Panels (**b**,**c**) show examples of Rietveld refinement for the selected $Mn_5Ge_{2.85}B_{0.15}$ and $Mn_{4.75}Co_{0.25}Ge_3$ alloys, respectively. The solid line through the experimental points represents a fitted model. The difference between the experimental and theoretical curves is represented by the bottom solid green curve.

The experimentally determined density (d) values were in good agreement with those obtained from the diffractogram analysis (see Table 1). The observed differences between the experimental and theoretical values resulted from the imperfections of the actual samples in the form of cracks or voids and were less than 6%. Density measurements allowed for the determination of the entropy change values in volumetric units (mJ cm^{-3} K^{-1}), which is more meaningful for design and construction purposes [64,65].

The EDS measurements were carried out at different spots along the samples. The refined average compositions for all the obtained samples are summarized in Table 1. The chemical composition ratio was in good agreement with the nominal one.

The temperature dependencies of the magnetic susceptibilities of these compounds in the ZFC mode and in the field of 0.1 T are shown in Figure 2. The magnetic transition temperatures (T_C) for each alloy were determined from the derivative of the ZFC magnetization (Figure 3a) and are given in Table 2. The T_C values for all tested alloys were smaller than for the parent compound (T_C = 295(1) K), except for the sample containing B, for which a 3 K increase in T_C was observed. The largest reduction in T_C was seen for the samples with Co (281(1) K) and Cr (288(1) (K)). The T_C values are in good agreement with those presented in the literature (see Table 5). In addition, for the sample $(Mn_{0.95}Co_{0.05})_5Ge_3$, the obtained T_C value was higher than that obtained by Kim et al. (T_C = 273 K) [42] and by Kang et al. (T_C = 266 K) [45]. These results suggest that the magnetic properties of Mn_5Ge_3 are sensitive to the synthesis conditions.

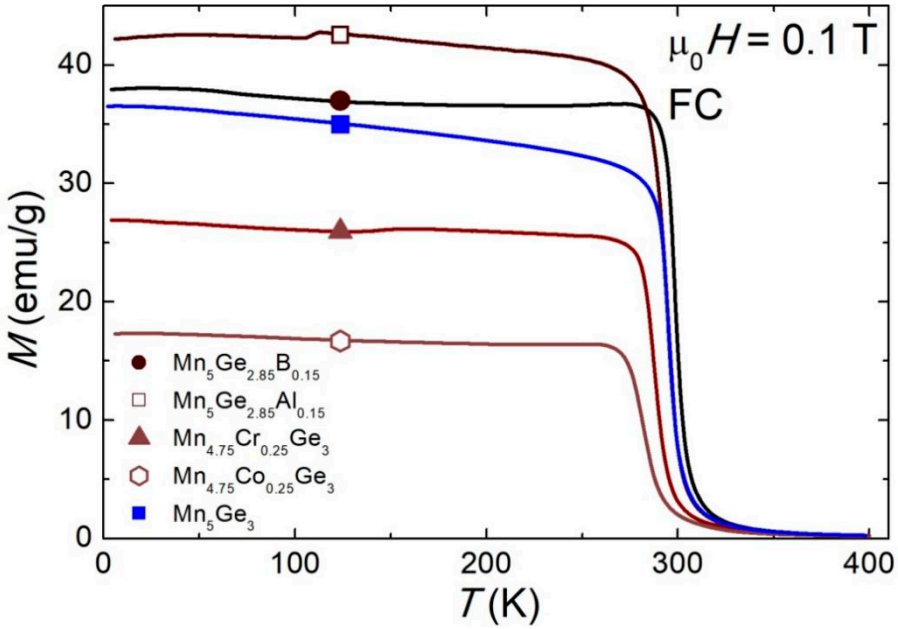

Figure 2. Temperature dependence of the field cooled (FC) magnetization of the $(Mn_{1-x}Me_x)_5(Ge_{1-y}Oe_y)_3$ alloys in the magnetic field of 0.1 T.

Table 2. The magnetic properties of the $(Mn_{1-x}Me_x)_5(Ge_{1-y}Oe_y)_3$ alloys: values of the magnetic Curie temperature (T_C), the paramagnetic Curie–Weiss temperature (Θ_{CW}), the effective magnetic moments (μ_{eff}) per Mn atom, and the saturation magnetization (σ_S) per Mn atom at 4 K.

Alloy	T_C (K)	Θ_{CW} (K)	μ_{eff} (μ_B/Mn)	σ_S (μ_B/Mn) at 4 K
Mn_5Ge_3	295(1)	307(1)	2.09(2)	2.60(8)
$Mn_5(Ge_{0.95}B_{0.05})_3$	298(1)	310(1)	1.86(3)	2.32(1)
$Mn_5(G_{e0.95}Al_{0.05})_3$	294(1)	304(1)	1.95(1)	2.57(7)
$(Mn_{0.95}Cr_{0.05})_5Ge_3$	288(1)	304(1)	1.90(2)	2.10(1)
$(Mn_{0.95}Co_{0.05})_5Ge_3$	281(1)	294(1)	1.96(5)	2.51(2)

The inverse susceptibility data (Figure 3b) were fitted with the Curie–Weiss (CW) law:

$$\chi = \frac{N_A \mu_{eff}^2}{3k_B(T - \Theta_{CW})}, \quad (1)$$

where μ_{eff} is the effective magnetic moment, and Θ_{CW} is the paramagnetic Curie–Weiss temperature. The effective magnetic moment per Mn ion was calculated and is provided in Table 2. Figure 3b indicates that above the ordering temperatures, the CW law was well obeyed. The values of μ_{eff} and Θ_{CW} estimated from the CW fit are also given in Table 2. For all alloys, the value of μ_{eff} was practically the same, approximately 2 μ_B. This value, as in many other materials containing Mn, was lower than the theoretical value for Mn^{2+} ion (5.92 μ_B) due to the influence of the crystal field [66]. For the pure Mn_5Ge_3, the value of $\mu_{\mu eff}$ was in good agreement with previous measurements [51,67]. The performed chemical modifications led to a small decrease in the μ_{eff} value compared to that of the pure sample. Moreover, the obtained μ_{eff} values were typical of other Mn-based alloys and compounds [68–70]. It was also observed that the used substitutions resulted in the lowering of Θ_{CW}. Similar magnetic behavior and changes in T_C and magnetization were found for other Mn_5Ge_3-based alloys [41,43,71].

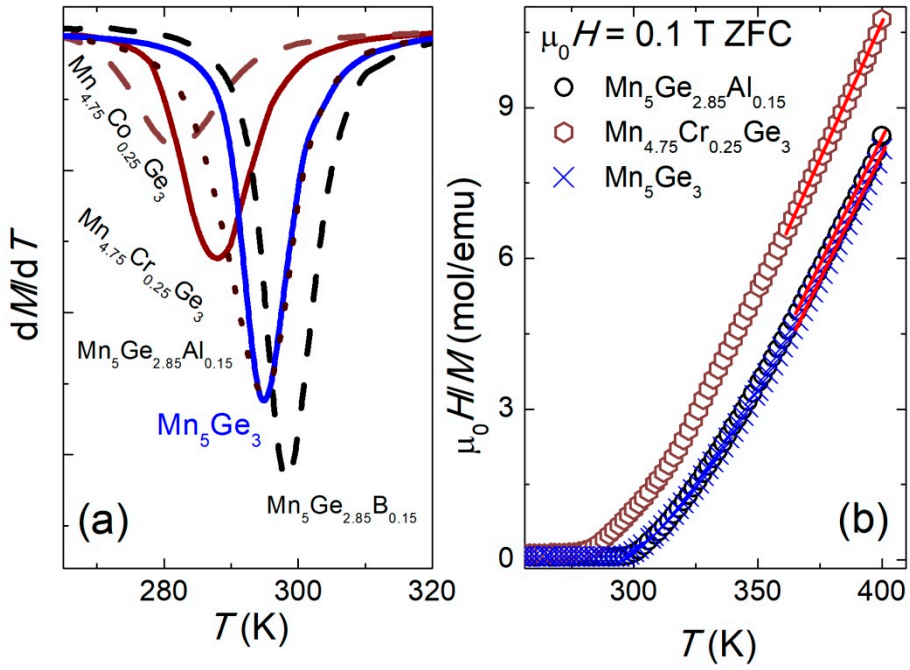

Figure 3. (**a**) The derivative of magnetization (dM/dT) versus temperature; (**b**) temperature dependence of $\mu_0 H/M$ between 260 and 400 K. The solid lines represent the fits of the Curie–Weiss law to the data between 360 and 400 K for selected compositions of the $(Mn_{1-x}Me_x)_5(Ge_{1-y}Oe_y)_3$ series.

Figure 4 shows the field dependence of the magnetization $\sigma(\mu_0 H)$ measured at T = 4 K. The values of the characteristic parameters for the starting compound Mn_5Ge_3, such as saturation magnetization (σ_S = 2.60(8) μ_B/Mn), saturation field ($\mu_0 H_S$ = 1.5(1) T), and coercivity field ($\mu_0 H_C$~10 mT), are in good agreement with literature values [72]. The value of σ_S decreased as a result of all the chemical composition changes made (see Table 2), consistent with results reported earlier [41,43,49,52]. On the other hand, a small amount of B or Al in the place of Ge reduced $\mu_0 H_S$ to 1.2(1) T, making these samples easier to magnetize. From the inset of Figure 4, it is evident that after the chemical modification no hysteresis loop appeared in the samples studied.

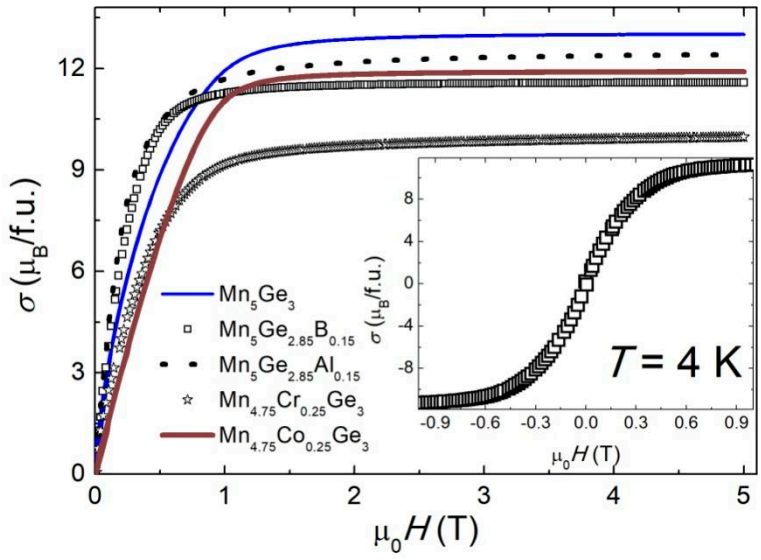

Figure 4. The first quadrant of the magnetization loop for $(Mn_{1-x}Me_x)_5(Ge_{1-y}Oe_y)_3$ alloys at 4 K. Inset: close-up of the weak-field range for the sample with B.

Figure 5 shows the Arrott plots [73] for the alloys with Co and Cr as examples. The positive slopes of the Arrott plots indicate that the paramagnetic (PM) to ferromagnetic (FM) transitions were of the second order.

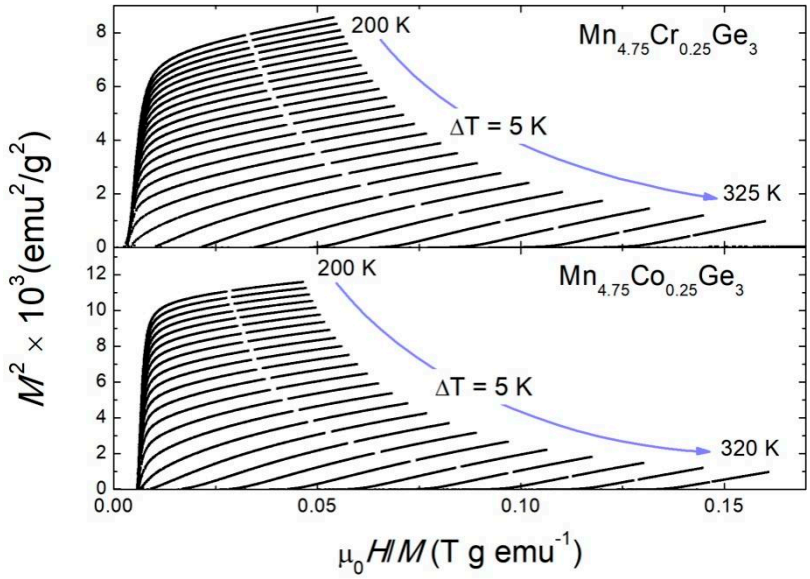

Figure 5. The Arrott plots, M^2 vs. $\mu_0 H/M$, measured in the temperature range around T_C for the selected samples.

To calculate the isothermal entropy change, ΔS_m, the standard Maxwell equation was used [3,5,74]:

$$\Delta S_m(T, \mu_0 H) = \int_0^{\mu_0 H} (\delta M/\delta T) dH. \quad (2)$$

The temperature dependencies of the ΔS_m calculated from $M(\mu_0 H)$ for different samples are presented in Figure 6. For all materials, $\Delta S_m(T)$ showed a negative value and the plot of this dependence took the shape of a symmetrical peak located at T_C. Such properties of the $\Delta S_m(T)$ curve are typical of materials showing a second-order phase transition from the PM to the FM state, which is in line with the analysis of the Arrott plots. The Mn_5Ge_3 parent compound showed the highest value of $|\Delta S_m|$ for a magnetic field change of 5 T as $|\Delta S_m|^{MAX}$ = 7.1(1) J kg^{-1} K^{-1} at 300(1) K. For the remaining materials, the $|\Delta S_m|^{MAX}$ value was lower (see Table 3). The greatest reduction was observed for the sample with Cr, for which the value of $|\Delta S_m|^{MAX}$ decreased by 32% compared to that of the starting material. On the other hand, for the Al sample, the $|\Delta S_m|^{MAX}$ value was only 4% lower than that of Mn_5Ge_3. The temperature at which the $|\Delta S_m|^{MAX}$ occurred also shifted towards lower values for modified materials. The exception was the sample with B for which the temperature of $|\Delta S_m|^{MAX}$ (T_{max} = 302(1) K) was higher than for the pure compound Mn_5Ge_3, as the T_C.

We also calculated the relative cooling power (RCP) according to the equation RCP = $|\Delta S_m|^{MAX} \times \Delta T_{FWHM}$, where ΔT_{FWHM} is the full-width at half-maximum of ΔS_m. RCP determines the amount of heat that can be transferred between cold and hot reservoirs and is one of the parameters determining the performance of magnetocaloric materials [1]. As with the $|\Delta S_m|^{MAX}$ value, the materials after the chemical modification showed lower RCP values than the original compound (see Table 3). This was mainly due to the lower $|\Delta S_m|^{MAX}$ value of these materials.

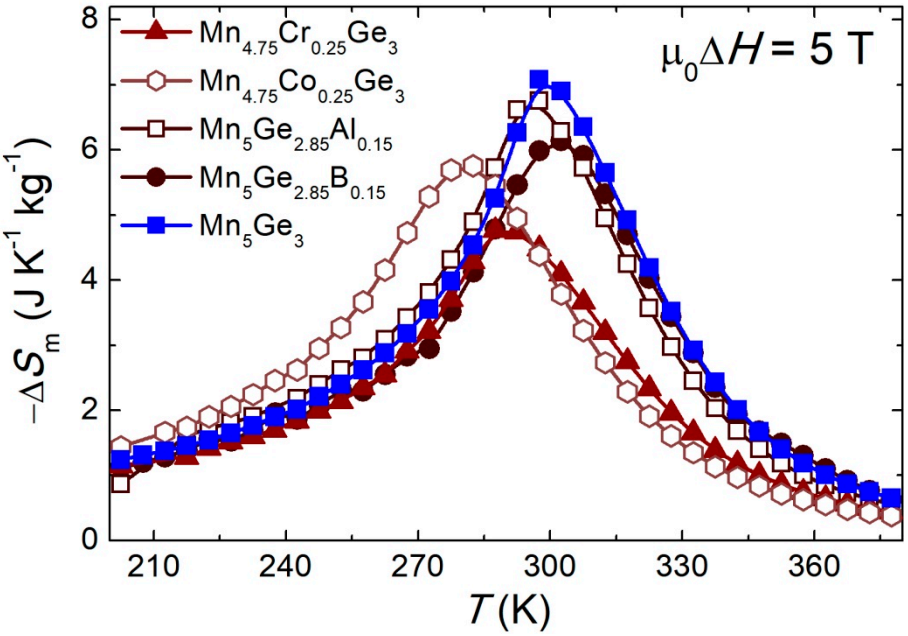

Figure 6. The entropy change ΔS_m vs. temperature for a magnetic field change $\mu_0\Delta H$ = 5 T for the $(Mn_{1-x}Me_x)_5(Ge_{1-y}Oe_y)_3$ alloys. The lines in the figure are a guide for the eye.

Table 3. Magnetocaloric performance of the $(Mn_{1-x}Me_x)_5(Ge_{1-y}Oe_y)_3$ alloys: the maximum entropy change ($|\Delta S_m|^{MAX}$) in mass (J kg^{-1} K^{-1}) and volumetric (mJ cm^{-3} K^{-1}) units, the adiabatic temperature change (ΔT_{ad}), the relative cooling power (RCP), and the temperature-averaged entropy change (TEC) for temperature lifts, ΔT_{lift} = 3, 5, and 10 K. The values of all the parameters were collected for different values of the magnetic field change ($\mu_0\Delta H$).

Alloy	$\mu_0\Delta H$ (T)	$\lvert\Delta S_m\rvert^{MAX}$ (J kg^{-1} K^{-1})	$\lvert\Delta S_m\rvert^{MAX}$ (mJ cm^{-3} K^{-1})	ΔT_{ad} (K)	RCP (J kg^{-1})	TEC(3) (J kg^{-1} K^{-1})	TEC(5) (J kg^{-1} K^{-1})	TEC(10) (J kg^{-1} K^{-1})
Mn_5Ge_3	5	7.1(1)	50(1)	-	390(6)	7.2(1)	7.2(1)	7.1(1)
	3	5.1(1)	36(1)	-	209(5)	5.1(1)	5.1(1)	4.9(1)
	1	2.3(1)	16(1)	1.1(1)	46(2)	2.3(1)	2.2(1)	2.1(1)
$Mn_5(Ge_{0.95}B_{0.05})_3$	5	6.2(1)	41(1)	-	366(7)	6.2(1)	6.2(1)	6.1(1)
	3	4.6(1)	31(1)	-	198(5)	4.6(1)	4.5(1)	4.4(1)
	1	2.2(1)	15(1)	1.2(1)	53(3)	2.2(1)	2.1(1)	2.0(1)
$Mn_5(Ge_{0.95}Al_{0.05})_3$	5	6.8(1)	47(1)	-	381(6)	6.8(1)	6.8(1)	6.7(1)
	3	4.7(1)	33(1)	-	212(5)	4.8(1)	4.8(1)	4.7(1)
	1	2.2(1)	15(1)	1.2(1)	57(3)	2.1(2)	2.1(1)	2.0(1)
$(Mn_{0.95}Cr_{0.05})_5Ge_3$	5	4.8(1)	33(1)	-	302(7)	4.8(1)	4.8(1)	4.7(1)
	3	3.4(1)	23(1)	-	160(5)	3.4(1)	3.3(1)	3.3(1)
	1	1.5(1)	10(1)	0.8(1)	39(3)	1.4(1)	1.4(1)	1.4(1)
$(Mn_{0.95}Co_{0.05})_5Ge_3$	5	5.8(1)	40(1)	-	365(7)	5.8(1)	5.8(1)	5.8(1)
	3	3.9(1)	27(1)	-	203(5)	3.9(1)	3.9(1)	3.8(1)
	1	1.4(1)	10(1)	0.8(1)	45(3)	1.4(1)	1.4(1)	1.4(1)

The RCP value is easy to calculate, which is why it is often reported in publications and makes it easier to compare the performance of individual magnetocaloric materials. However, as it is determined for a wide range of temperatures, it is of little use in the construction of specific devices. Therefore, another magnetocaloric parameter called temperature averaged entropy change (TEC) has been proposed [75]. The value of the TEC was calculated using the formula [75]:

$$\mathrm{TEC}(\Delta T_{lift}) = \frac{1}{\Delta T_{lift}} \max_{T_{mid}} \left\{ \int_{T_{mid}-\Delta T_{lift}/2}^{T_{mid}+\Delta T_{lift}/2} \Delta S_m(T)dT \right\}, \quad (3)$$

where ΔT_{lift} and T_{mid} denote the temperature lift and averaged temperature, respectively. The values of TEC for ΔT_{lift} equal to 3, 5, and 10 K for the studied materials are collected in Table 3. For individual materials, the TEC values were close to the maximum $|\Delta S_m|^{MAX}$ value for a given value of $\mu_0\Delta H$. This behavior is typical of materials with a second-order phase transition [75].

The dependencies of $|\Delta S_m|^{MAX}$, RCP, and TEC(5) on the magnetic field change $\mu_0\Delta H$ are plotted in Figure 7. From these graphs, one can read the value of the magnetocaloric parameters for any value of $\mu_0\Delta H$. For all parameters, we observed the power-type dependence $\sim\mu_0\Delta H^n$. From the fitting of the $|\Delta S_m|^{MAX}$ and RCP data, the values of the critical exponents could be determined with the following relations: $|\Delta S_m|^{MAX}(\mu_0\Delta H) \sim \mu_0\Delta H^{(1+(1/\delta)(1-1/\beta))}$ and RCP$(\mu_0\Delta H) \sim \mu_0\Delta H^{(1+1/\delta)}$ [76]. At first, from the relation RCP$(\mu_0\Delta H)$, we determined the value of $\delta = 1/(n-1)$. Then, using the obtained value of δ and the parameter of the fit determined from the relation $|\Delta S_m|^{MAX}(\mu_0\Delta H) \sim \mu_0\Delta H^n$, the value of β was calculated according to the formula $\beta = 1/(1-\delta(n-1))$. The obtained exponents β, δ, and n (for $|\Delta S_m|^{MAX}(\mu_0\Delta H)$) and their expected values based on the relevant theoretical models are collected in Table 4. For $Mn_5(Ge_{0.95}B_{0.05})_3$, $Mn_5(Ge_{0.95}Al_{0.05})_3$, and $(Mn_{0.95}Co_{0.05})_5Ge_3$, the obtained values of n and δ were closest to the 3D Heisenberg model, while for the Mn_5Ge_3 and $(Mn_{0.95}Cr_{0.05})_5Ge_3$ alloys, they were closest to the mean-field model [77]. For TEC(5), the values of the critical exponent were very similar to those obtained for $|\Delta S_m|^{MAX}$ and equal to 0.72(2), 0.67(2), 0.72(2), 0.75(2), and 0.86(3) for Mn_5Ge_3, $Mn_5Ge_{2.85}B_{0.15}$, $Mn_5Ge_{2.85}Al_{0.15}$, $Mn_{4.75}Cr_{0.25}Ge_3$, and $Mn_{4.75}Co_{0.25}Ge_3$, respectively.

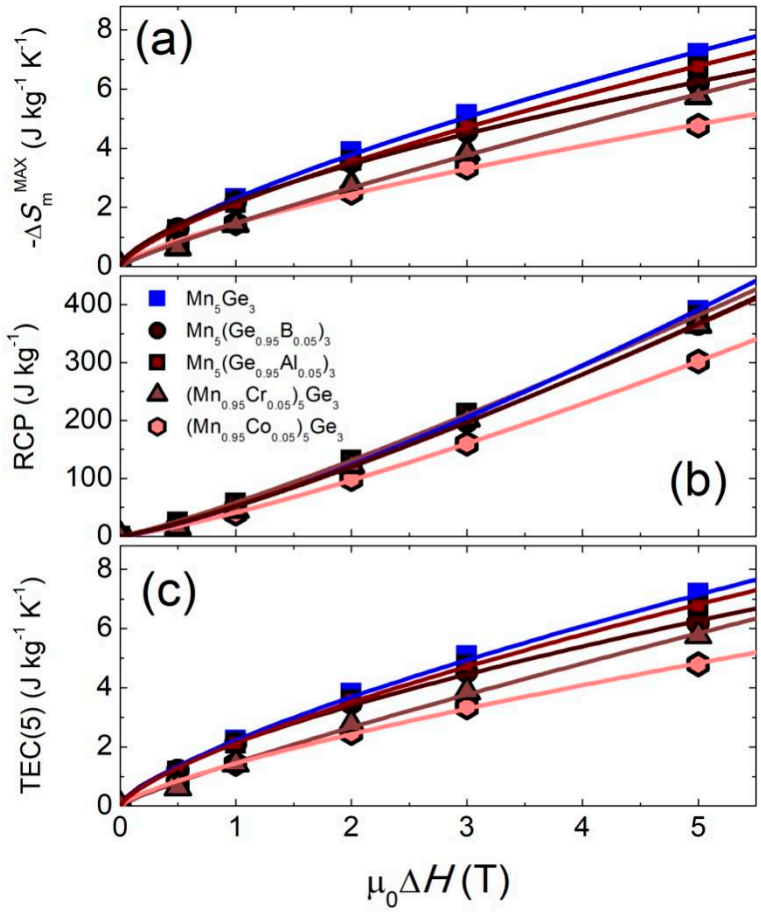

Figure 7. (**a**) The curves of ΔS_m vs. $\mu_0\Delta H$; (**b**) RCP vs. $\mu_0\Delta H$; (**c**) TEC(5) vs. $\mu_0\Delta H$ for the $(Mn_{1-x}Me_x)_5(Ge_{1-y}Oe_y)_3$ alloys. The lines show the results of the fit with the $\sim\mu_0\Delta H^n$-type dependency, where n is a critical exponent.

Table 4. The critical exponent values β, δ, and n for the $(Mn_{1-x}Me_x)_5(Ge_{1-y}Oe_y)_3$ alloys.

	β	δ	n
Heisenberg model	0.365	4.807	0.626
Ising model	0.325	4.815	0.568
Mean-field	0.5	3	0.66
Tricritical mean-field model	0.25	5	0.40
Mn_5Ge_3	0.48(4)	3.8(3)	0.71(2)
$Mn_5(Ge_{0.95}B_{0.05})_3$	0.38(2)	4.8(2)	0.65(2)
$Mn_5(G_{e0.95}Al_{0.05})_3$	0.38(2)	5.9(3)	0.72(1)
$(Mn_{0.95}Cr_{0.05})_5Ge_3$	0.48(3)	4.2(2)	0.74(2)
$(Mn_{0.95}Co_{0.05})_5Ge_3$	0.61(9)	4.5(8)	0.86(3)

Table 3 summarizes the magnetocaloric properties of all the studied alloys. No enhancement of the magnetocaloric effect was observed for any of the samples tested when the chemical composition of the Mn_5Ge_3 was modified by 5%.

To gain more information about the magnetocaloric properties of the $(Mn_{1-x}Me_x)_5(Ge_{1-y}Oe_y)_3$ alloys, the phenomenological universal curve can be constructed by normalizing the entropy change to $\Delta S' = \Delta S_m/\Delta S_m{}^{MAX}$ and rescaling the temperature axis below and above T_C:

$$\theta = \begin{cases} -\frac{T-T_C}{T_{r1}-T_C}, & T \leq T_C \\ \frac{T-T_C}{T_{r2}-T_C}, & T > T_C \end{cases}, \quad (4)$$

where T_{r1} and T_{r2} are the temperatures at which $\Delta S_m = \Delta S_m{}^{MAX}/2$ [76]. Figure 8 shows the θ dependence of $\Delta S'$ for a magnetic field change of 5 T. The peaks of the curves collapsed onto the same universal curve, which is associated with the FM ordering transition of the second order and reveals a universal behavior of the $(Mn_{1-x}Me_x)_5(Ge_{1-y}Oe_y)_3$ alloys. Similar results have been obtained in other studies [37,38].

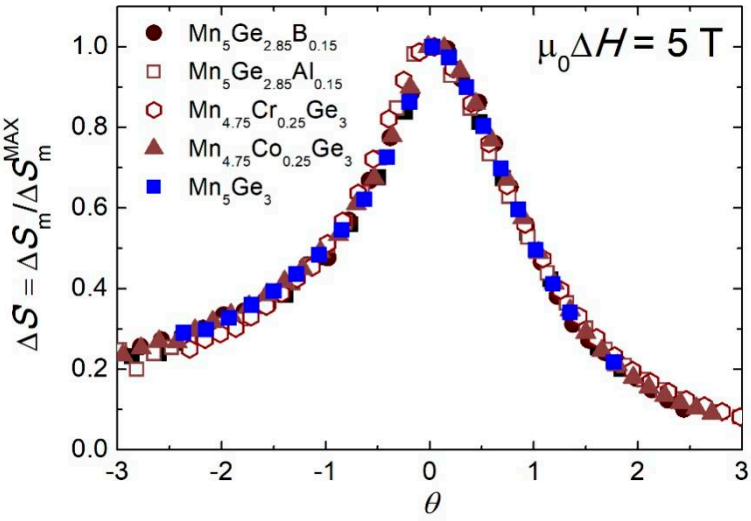

Figure 8. Magnetocaloric universal curves of the $(Mn_{1-x}Me_x)_5(Ge_{1-y}Oe_y)_3$ alloys for a magnetic field change of 5 T.

Additionally, the specific heat (C_p) data (Figure 9) were used to calculate the adiabatic temperature change $\Delta T_{ad} = -\Delta S_m \times T/C_p$ [78]. For this purpose, the maximum value of $-\Delta S_m$ and the C_p value at T_C were used. The obtained values of the magnetocaloric parameters are summarized in Table 3. For all samples, the ΔT_{ad} value fluctuated around 1 K for $\mu_0\Delta H$ = 1 T. For the samples with Al and B, the ΔT_{ad} value was slightly higher (by ~0.1 K) than for pure Mn_5Ge_3, but the difference was within the estimated measurement error. For the samples containing Cr and Co, the values of ΔT_{ad} were clearly lower but in

line with previous results of direct measurements by Kang et al. [45]. Thus, for all of the abovementioned chemical modifications, the decrease in the ΔT_{ad} value was due to the blurring of the magnetic transition and lower magnetic entropy.

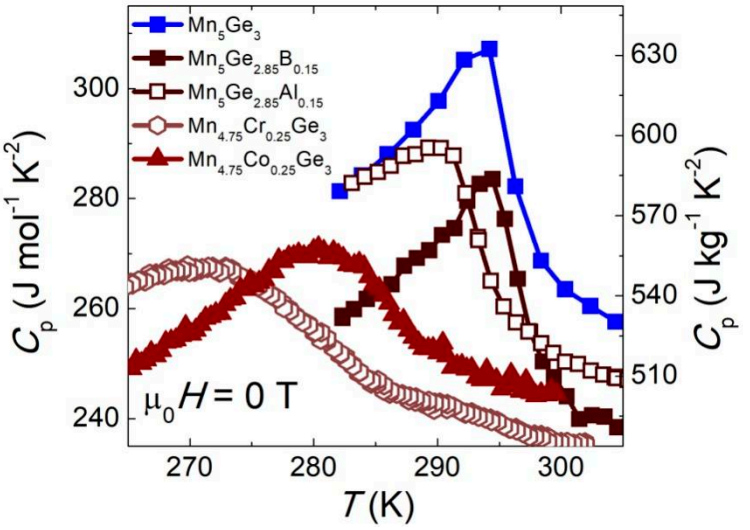

Figure 9. Specific heat vs. temperature near the phase transition of the studied $(Mn_{1-x}Me_x)_5(Ge_{1-y}Oe_y)_3$ samples. The lines in the figure are a guide for the eye.

For some composites, an enhancement of the magnetocaloric properties was observed [79]. Therefore, we calculated the magnetic entropy change for an exemplary composite according to the equation: $\Delta S_m{}^{comp}(T) = (1 - z)\Delta S_m{}^{I}(T) + z\Delta S_m{}^{II}(T)$, where $\Delta S_m{}^{I}(T)$ and $\Delta S_m{}^{II}(T)$ represent the experimental data for the composite components. In Figure 10, the calculated result (for selected $z = 0.4$ value) is compared with the experimental data for the Mn_5Ge_3 and $(Mn_{0.95}Co_{0.05})_5Ge_3$ samples. Although the maximum value of ΔS_m was reduced to ~5 J kg^{-1} K^{-1}, the composite sample showed a broad table-like magnetocaloric effect in a wide temperature range. Therefore, the RCP value was enhanced in this case up to 405(9) J kg^{-1}, and the magnetocaloric properties were improved.

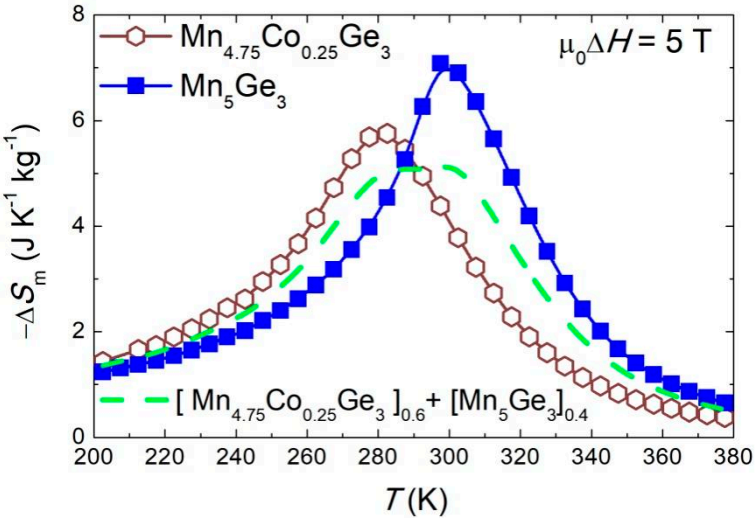

Figure 10. The calculated temperature dependence of the magnetic entropy change ΔS_m for the $((Mn_{0.095}Co_{0.05})_5Ge_3)_{0.6}(Mn_5Ge_3)_{0.4}$ composite material (dashed line) compared with the results for its constituent compounds. The results are presented for a magnetic field change of 5 T. The solid lines in the figure are a guide for the eye.

Finally, we summarize the present and literature data for the Mn_5Ge_3 and Mn_5Ge_3-based alloys. In Table 5, the values of the ordering temperature (T_C), the maximum entropy change ($|\Delta S_m|^{MAX}$), and the relative cooling power (RCP) for a magnetic field change of 1 T and 2 T are collected. We chose the $|\Delta S_m|^{MAX}$ and RCP values for a field changes of 1 T and 2 T because they are most often presented in the publications and are the closest to the values of the magnetic field changes that can be used in actual devices. In addition, Figure 11 shows a graph with the $|\Delta S_m|^{MAX}$ values (for a magnetic field change of 2 T) as a function of T_C for various samples of the Mn_5Ge_3 compound and its alloys. The data were divided into groups according to the type of element modifying the chemical composition. This graph clearly shows that by using an appropriate modification of the chemical composition, it is possible to significantly expand the operating range of the magnetocaloric material based on Mn_5Ge_3; a practically constant value of $|\Delta S_m|^{MAX} \approx 3.5$ J kg^{-1} K^{-1} can be achieved in the range from 280 to 303 K. The graph also shows a clear trend of changes in the magnetocaloric properties due to the modification of the chemical composition. The points are arranged in a convex arc that has an extremity that is determined by the pure Mn_5Ge_3 compound. By substituting different chemical elements, we can modify the T_C. For example, the addition of Ni in the place of Mn leads to a lower T_C, while the addition of Sb in place of Ge can increase the T_C. The second important conclusion is that the $|\Delta S_m|^{MAX}$ value did not increase as a result of the known chemical composition modifications. In practice, the $|\Delta S_m|^{MAX}$ value for Mn_5Ge_3-based alloys is always lower than for the parent compound. In a few cases, the observed increased $|\Delta S_m|^{MAX}$ value may result from measurement errors not included in the calculation. The collected data also show how the parameter values are distributed for Mn_5Ge_3 samples obtained by different authors. The T_C values range between 293 and 300 K, $|\Delta S_m|^{MAX}$ values (for $\mu_0\Delta H = 2$ T) range from 3.6 to 4.1 J kg^{-1} K^{-1}, and RCP values (for $\mu_0\Delta H = 2$ T) range from 100 to 145 J kg^{-1}. These differences result from different microstructural properties of different samples such as slightly different stoichiometries, different crystallites size, and different shapes of the sample for magnetic measurements. Figure 11 can be used as a signpost for further research on the improvement of the magnetocaloric properties of the Mn_5Ge_3 compound in terms of chemical composition modification.

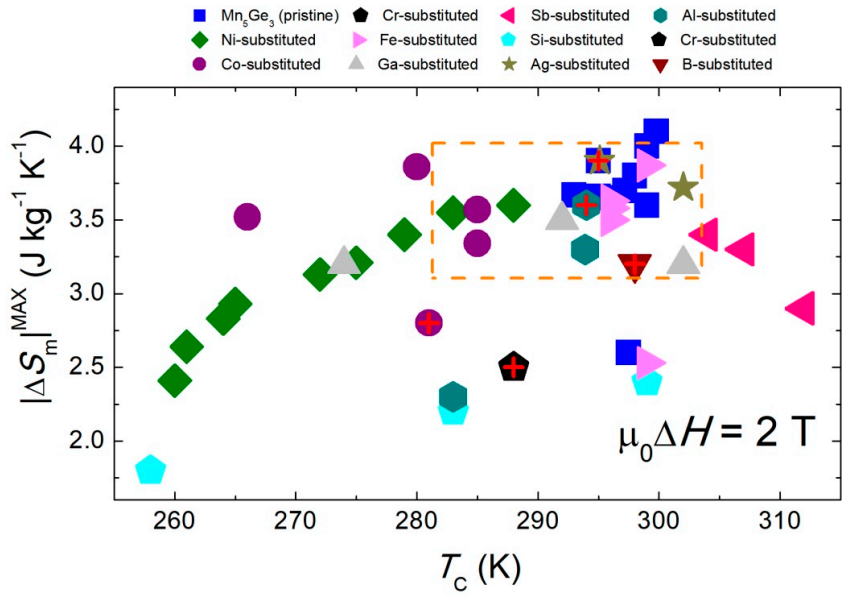

Figure 11. Maximum values of magnetic entropy change $|\Delta Sm|^{MAX}$ for different samples of Mn5Ge3 and Mn5Ge3-based alloys for a magnetic field change of 2 T taken from the literature (see Table 4). In the graph, the data for Mn5Ge3-based alloys are grouped according to the type of the substituted chemical element. The values obtained for the samples of the present work are marked with red crosses. The symbols within the rectangle correspond to the samples with an almost constant $|\Delta Sm|^{MAX}$ value in a wide temperature range.

Table 5. The ordering temperature (T_C), the maximum entropy change ($|\Delta S_m|^{MAX}$), and the relative cooling power (RCP) for a 1 T and 2 T magnetic field change for Mn_5Ge_3 and Mn_5Ge_3-based alloys.

Alloy	T_C (K)	$\mu_0\Delta H$ (T)	$\lvert\Delta S_m\rvert^{MAX}$ (J kg^{-1} K^{-1})	RCP (J kg^{-1})	References
Mn_5Ge_3	295(1)	1	2.3(1)	46(2)	This work
		2	3.9(1)	125(1)	This work
Mn_5Ge_3	295	1	2.06	-	[43]
		2	3.66	-	[43]
Mn_5Ge_3	293	1	2.5	43	[71]
Mn_5Ge_3	293	1	2.21	-	[48]
		2	3.67	125	[48]
Mn_5Ge_3	296	2	3.65	-	[47]
Mn_5Ge_3	298	2	3.8	133	[52]
Mn_5Ge_3	297.2	2	3.7	-	[53]
		1	2.3	-	[53]
Mn_5Ge_3	299.8	1	2.6	-	[55]
		2	4.1	-	[55]
Mn_5Ge_3	296	1	2.5 ($\parallel c$ axis)	-	[39]
		1	2.15 ($\perp c$ axis)	-	[39]
Mn_5Ge_3	299	1	2.6 ($\parallel c$ axis)	-	[40]
		1	2.0 ($\perp c$ axis)	-	[40]
		2	4.0 ($\parallel c$ axis)	145	[40]
		2	3.6 ($\perp c$ axis)	104	[40]
$Mn_{4.9}Ge_{3.1}$	281	1	1.91	46	[41]
Mn_5Ge_3	290	1	2.38	48	[41]
$Mn_{5.1}Ge_{2.9}$	302	1	2.91	58	[41]
Mn_5Ge_3 (thin film)	-	1	1.59	64	[80]
Mn_5Ge_3 (thin film)	-	1	1.75	81	[80]
			$(Mn_{1-x}Me_x)_5Ge_3$		
$Mn_{4.75}Cr_{0.25}Ge_3$	288(1)	1	1.5 (1)	39(1)	This work
		2	2.5(1)	99(1)	This work
$Mn_{4.95}Fe_{0.05}Ge_3$	296	2	3.58	-	[47]
$Mn_{4.9}Fe_{0.1}Ge_3$	296	2	3.50	-	[47]
$Mn_{4.85}Fe_{0.15}Ge_3$	296	2	3.63	-	[47]
$Mn_{4.75}Fe_{0.25}Ge_3$	299	2	3.87	130	[44]
$Mn_{4.75}Fe_{0.25}Ge_3$	311	1	1.59	42	[42]
$Mn_4Fe_1Ge_3$	320	2	3.1	-	[57]
$Mn_{4.95}Co_{0.05}Ge_3$	285	1	1.85		[43]
		2	3.34	-	[43]
$Mn_{4.1}Co_{0.1}Ge_3$	285	1	2.00	-	[43]
		2	3.57	-	[43]
$Mn_{4.85}Co_{0.15}Ge_3$	280	1	2.15	-	[43]
		2	3.86	-	[43]
$Mn_{4.75}Co_{0.25}Ge_3$	281(1)	1	1.4(1)	45(1)	This work
		2	2.8(1)	122(1)	This work
$Mn_{4.75}Co_{0.25}Ge_3$	266	2	3.52	136	[44]
$Mn_{4.75}Co_{0.25}Ge_3$	273	1	2.81	43	[42]
$Mn_{4.95}Ni_{0.05}Ge_3$	285	1	2.2	53	[71]
$Mn_{4.95}Ni_{0.05}Ge_3$	283	1	2.13	-	[48]
		2	3.55	135	[48]
$Mn_{4.925}Ni_{0.075}Ge_3$	279	1	2.02	-	[48]
		2	3.40	130	[48]
$Mn_{4.9}Ni_{0.1}Ge_3$	275	1	1.91	-	[48]
		2	3.21	132	[48]
$Mn_{4.9}Ni_{0.1}Ge_3$	268	1	1.2	49	[71]

Table 5. *Cont.*

Alloy	T_C (K)	$\mu_0\Delta H$ (T)	$\lvert\Delta S_m\rvert^{MAX}$ (J kg^{-1} K^{-1})	RCP (J kg^{-1})	References
$Mn_{4.875}Ni_{0.125}Ge_3$	272	1	1.83	-	[48]
		2	3.13	138	[48]
$Mn_{4.85}Ni_{0.15}Ge_3$	265	1	1.72	-	[48]
		2	2.93	129	[48]
$Mn_{4.8}Ni_{0.2}Ge_3$	264	1	1.64	-	[48]
		2	2.83	130	[48]
$Mn_{4.75}Ni_{0.25}Ge_3$	261	1	1.57	-	[48]
		2	2.64	124	[48]
$Mn_{4.975}Ni_{0.025}Ge_3$	288	1	2.20	-	[48]
		2	3.60	130	[48]
$Mn_{4.6}Ni_{0.4}Ge_3$	260	1	1.38	-	[48]
		2	2.41	-	[48]
$Mn_5(Ge_{1-y}Oe_y)_3$					
$Mn_5Ge_{2.85}B_{0.15}$	298(1)	1	2.2(1)	53(1)	This work
		2	3.5(1)	121(1)	This work
$Mn_5G_{e2.85}Al_{0.15}$	294(1)	1	2.2(1)	57(1)	This work
		2	3.6(1)	131(1)	This work
$Mn_5Ge_{2.5}Al_{0.5}$	293.9	1	2.0	-	[53]
		2	3.3	-	[53]
$Mn_5Ge_2Al_1$	283.0	1	1.4	-	[53]
		2	2.3	-	[53]
$Mn_5Ge_{2.5}Si_{0.5}$	299	2	2.4	-	[50]
$Mn_5Ge_{2.0}Si_{1.0}$	283	2	2.2	-	[50]
$Mn_5Ge_{1.5}Si_{1.5}$	258	2	1.8	-	[50]
$Mn_5Ge_{1.0}Si_{2.0}$	198	2	1.7	-	[50]
$Mn_5Ge_{2.9}Fe_{0.1}$	299	2	2.53	88	[56]
$Mn_5Ge_{2.7}Ga_{0.3}$	302	2	3.2	112	[51]
$Mn_5Ge_{2.4}Ga_{0.6}$	292	2	3.5	123	[51]
$Mn_5Ge_{2.1}Ga_{0.9}$	274	2	3.2	128	[51]
$Mn_5Ge_{2.9}Ag_{0.1}$	302	2	3.72	123.1	[54]
$Mn_5Ge_{2.9}Ag_{0.1}$	295.1	1	2.5	-	[55]
		2	3.9	-	[55]
$Mn_5Ge_{2.9}Sb_{0.1}$	304	2	3.4	129.2	[52]
$Mn_5Ge_{2.8}Sb_{0.2}$	307	2	3.3	125.4	[52]
$Mn_5Ge_{2.7}Sb_{0.3}$	312	2	2.9	127.6	[52]
$(Mn_{1-x}Me_x)_5(Ge_{1-y}Oe_y)_3$					
$Mn_4Fe_1Ge_{2.8}Si_{0.2}$	320	2	3.4	-	[57]
$Mn_4Fe_1Ge_{2.4}Si_{0.6}$	319	2	2.9	-	[57]
$Mn_4Fe_1Ge_2Si$	318	2	2.0	-	[57]
$Mn_{4.4}Fe_{0.6}GeSi_2$	182	2	1.9	-	[58]
$Mn_{4.3}Fe_{0.7}GeSi_2$	200	2	3.5	-	[58]
$Mn_{4.2}Fe_{0.8}GeSi_2$	196	2	3.7	211	[58]
$Mn_{4.1}Fe_{0.9}GeSi_2$	211	2	2.7	192	[58]

4. Conclusions

In this work, the effect of chemical composition modification on the magnetocaloric properties of Mn_5Ge_3 was investigated. The following samples were prepared by induction melting: Mn_5Ge_3, $Mn_5(Ge_{0.95}B_{0.05})_3$, $Mn_5(Ge_{0.95}Al_{0.05})_3$, $(M_{n0.95}Cr_{0.05})_5Ge_3$, and $(Mn_{0.95}Co_{0.05})_5Ge_3$. The X-ray diffraction measurements revealed that the tested materials crystallized in the same hexagonal crystal structure (space group $P6_3/mcm$, No. 193) as the parent Mn_5Ge_3 compound. According to the magnetic measurements, all the studied compositions show soft ferromagnetic properties at room temperature. Modification of the chemical composition changed the Curie temperature from T_C = 295(1) K for the starting compound to 298(1), 294(1), 288(1), and 281(1) K for the alloys with 5% of B, Al, Cr, and

Co, respectively. The magnetic entropy change, characterizing the magnetocaloric effect, was reduced from $-\Delta S_m$ = 7.1(1) J kg^{-1} K^{-1} for the starting material to 6.2(1), 6.8(1), 4.8(1), and 5.8(1) J kg^{-1} K^{-1} for the alloys with B, Al, Cr, and Co substitution, respectively. For the samples with Al and B, the adiabatic temperature change ΔT_{ad} value was practically the same as for the parent compound, i.e., 1.1(1) K (for a magnetic field change of 1 T). However, for the samples with Co and Cr, the value of ΔT_{ad} decreased by 27%, i.e., down to 0.8(1) K. For all the performed chemical composition modifications, the RCP values were also reduced. Therefore, there was no enhancement of the magnetocaloric properties in the studied materials. The prepared samples fit well with the general trend of changes in the magnetocaloric properties of the Mn_5Ge_3 compound as a result of the modification of its chemical composition. Analysis of the literature data showed that appropriate modification of the chemical composition makes it possible to obtain a set of alloys with very similar magnetocaloric properties over a wide temperature range (i.e., 280–303 K). Therefore, a promising track to improve the MCE performance seems to be preparation of composites. An exemplary simulation of the $((Mn_{0.095}Co_{0.05})_5Ge_3)_{0.6}(Mn_5Ge_3)_{0.4}$ composite based on the experimentally measured components built a broad table-like magnetocaloric effect that improved the relative cooling power by 4%.

Author Contributions: Conceptualization, K.S. and T.T.; methodology, K.S., K.U., P.S. and H.G.; validation, K.S., K.U., P.S. and T.T.; formal analysis, K.S.; investigation, K.S., K.U., P.S. and H.G.; resources, T.T.; data curation, K.S.; writing—original draft preparation, K.S.; writing—review and editing, K.S., K.U., H.G., P.S. and T.T.; visualization, K.S.; supervision, T.T.; project administration, K.S. and T.T.; funding acquisition, T.T. All authors have read and agreed to the published version of the manuscript.

Funding: This research received no external funding.

Acknowledgments: The authors thank Daria Szewczyk for the technical support.

Conflicts of Interest: The authors declare no conflict of interest.

References

1. Franco, V.; Blázquez, J.S.; Ingale, B.; Conde, A. The Magnetocaloric Effect and Magnetic Refrigeration Near Room Temperature: Materials and Models. *Annu. Rev. Mater. Res.* **2012**, *42*, 305–342. [CrossRef]
2. Barclay, J.A. Magnetic Refrigeration: A Review of a Developing Technology. In *Advances in Cryogenic Engineering*; Fast, R.W., Ed.; A Cryogenic Engineering Conference Publication; Springer: Boston, MA, USA, 1988; Volume 33, pp. 719–731, ISBN 978-1-4613-9876-9.
3. Franco, V.; Blázquez, J.S.; Ipus, J.J.; Law, J.Y.; Moreno-Ramírez, L.M.; Conde, A. Magnetocaloric Effect: From Materials Research to Refrigeration Devices. *Prog. Mater. Sci.* **2018**, *93*, 112–232. [CrossRef]
4. Gottschall, T.; Skokov, K.P.; Fries, M.; Taubel, A.; Radulov, I.; Scheibel, F.; Benke, D.; Riegg, S.; Gutfleisch, O. Making a Cool Choice: The Materials Library of Magnetic Refrigeration. *Adv. Energy Mater.* **2019**, *9*, 1901322. [CrossRef]
5. Dzekan, D.; Waske, A.; Nielsch, K.; Fähler, S. Efficient and Affordable Thermomagnetic Materials for Harvesting Low Grade Waste Heat. *APL Mater.* **2021**, *9*, 011105. [CrossRef]
6. Brown, G.V. Magnetic Heat Pumping near Room Temperature. *J. Appl. Phys.* **1976**, *47*, 3673–3680. [CrossRef]
7. Synoradzki, K.; Nowotny, P.; Skokowski, P.; Toliński, T. Magnetocaloric Effect in $Gd_5(Si,Ge)_4$ Based Alloys and Composites. *J. Rare Earths* **2019**, *37*, 1218–1223. [CrossRef]
8. Pecharsky, V.K.; Gschneidner, K.A., Jr. Giant Magnetocaloric Effect in $Gd_5(Si_2Ge_2)$. *Phys. Rev. Lett.* **1997**, *78*, 4494–4497. [CrossRef]
9. Provenzano, V.; Shapiro, A.J.; Shull, R.D. Reduction of Hysteresis Losses in the Magnetic Refrigerant $Gd_5Ge_2Si_2$ by the Addition of Iron. *Nature* **2004**, *429*, 853–857. [CrossRef]
10. Annaorazov, M.P.; Nikitin, S.A.; Tyurin, A.L.; Asatryan, K.A.; Dovletov, A.K. Anomalously High Entropy Change in FeRh Alloy. *J. Appl. Phys.* **1996**, *79*, 1689–1695. [CrossRef]
11. Chirkova, A.; Skokov, K.P.; Schultz, L.; Baranov, N.V.; Gutfleisch, O.; Woodcock, T.G. Giant Adiabatic Temperature Change in FeRh Alloys Evidenced by Direct Measurements under Cyclic Conditions. *Acta Mater.* **2016**, *106*, 15–21. [CrossRef]
12. Gozdur, R.; Gębara, P.; Chwastek, K. A Study of Temperature-Dependent Hysteresis Curves for a Magnetocaloric Composite Based on La(Fe, Mn, Si)$_{13}$-H Type Alloys. *Energies* **2020**, *13*, 1491. [CrossRef]
13. Gębara, P.; Pawlik, P. Broadening of Temperature Working Range in Magnetocaloric La(Fe,Co,Si)$_{13}$-Based Multicomposite. *J. Magn. Magn. Mater.* **2017**, *442*, 145–151. [CrossRef]
14. Pathak, A.K.; Khan, M.; Dubenko, I.; Stadler, S.; Ali, N. Large Magnetic Entropy Change in $Ni_{50}Mn_{50-x}In_x$ Heusler Alloys. *Appl. Phys. Lett.* **2007**, *90*, 262504. [CrossRef]

15. Planes, A.; Mañosa, L.; Acet, M. Magnetocaloric Effect and Its Relation to Shape-Memory Properties in Ferromagnetic Heusler Alloys. *J. Phys. Condens. Matter* **2009**, *21*, 233201. [CrossRef] [PubMed]
16. Tegus, O.; Brück, E.; Buschow, K.H.J.; de Boer, F.R. Transition-Metal-Based Magnetic Refrigerants for Room-Temperature Applications. *Nature* **2002**, *415*, 150–152. [CrossRef]
17. Wada, H.; Tanabe, Y. Giant Magnetocaloric Effect of $MnAs_{1-x}Sb_x$. *Appl. Phys. Lett.* **2001**, *79*, 3302–3304. [CrossRef]
18. Zhang, H.; Gimaev, R.; Kovalev, B.; Kamilov, K.; Zverev, V.; Tishin, A. Review on the Materials and Devices for Magnetic Refrigeration in the Temperature Range of Nitrogen and Hydrogen Liquefaction. *Phys. B Condens. Matter* **2019**, *558*, 65–73. [CrossRef]
19. Ćwik, J.; Koshkid'ko, Y.; Nenkov, K.; Mikhailova, A.; Małecka, M.; Romanova, T.; Kolchugina, N.; de Oliveira, N.A. Experimental and Theoretical Analysis of Magnetocaloric Behavior of $Dy_{1-x}Er_xNi_2$ Intermetallics (x = 0.25, 0.5, 0.75) and Their Composites for Low-Temperature Refrigerators Performing an Ericsson Cycle. *Phys. Rev. B* **2021**, *103*, 214429. [CrossRef]
20. Ćwik, J.; Koshkid'ko, Y.; Małecka, M.; Weise, B.; Krautz, M.; Mikhailova, A.; Kolchugina, N. Magnetocaloric Prospects of Mutual Substitutions of Rare-Earth Elements in Pseudobinary $Tb_{1-x}Ho_xNi_2$ Compositions (x = 0.25–0.75). *J. Alloy. Compd.* **2021**, *886*, 161295. [CrossRef]
21. Andreenko, A.S.; Belov, K.P.; Nikitin, S.A.; Tishin, A.M. Magnetocaloric Effects in Rare-Earth Magnetic Materials. *Sov. Phys. Uspekhi* **1989**, *32*, 649–664. [CrossRef]
22. Kuz'min, M.D.; Tishin, A.M. Magnetic Refrigerants for the 4.2-20 K Region: Garnets or Perovskites? *J. Phys. D Appl. Phys.* **1991**, *24*, 2039–2044. [CrossRef]
23. Gschneidner, K.A.; Pecharsky, V.K. Rare Earths and Magnetic Refrigeration. *J. Rare Earths* **2006**, *24*, 641–647. [CrossRef]
24. Li, L.; Yan, M. Recent Progresses in Exploring the Rare Earth Based Intermetallic Compounds for Cryogenic Magnetic Refrigeration. *J. Alloy. Compd.* **2020**, *823*, 153810. [CrossRef]
25. Brück, E.; Tegus, O.; Cam Thanh, D.T.; Trung, N.T.; Buschow, K.H.J. A Review on Mn Based Materials for Magnetic Refrigeration: Structure and Properties. *Int. J. Refrig.* **2008**, *31*, 763–770. [CrossRef]
26. Phan, M.-H.; Yu, S.-C. Review of the Magnetocaloric Effect in Manganite Materials. *J. Magn. Magn. Mater.* **2007**, *308*, 325–340. [CrossRef]
27. Dubenko, I.; Khan, M.; Pathak, A.K.; Gautam, B.R.; Stadler, S.; Ali, N. Magnetocaloric Effects in Ni–Mn–X Based Heusler Alloys with X = Ga, Sb, In. *J. Magn. Magn. Mater.* **2009**, *321*, 754–757. [CrossRef]
28. Chaudhary, V.; Chen, X.; Ramanujan, R.V. Iron and Manganese Based Magnetocaloric Materials for near Room Temperature Thermal Management. *Prog. Mater. Sci.* **2019**, *100*, 64–98. [CrossRef]
29. Wrzeciono, A.; Gemperle, R. Abhängigkeit der Bereichsstruktur in Mn_5Ge_3 von der Kristalldicke. *Phys. Status Solidi (B)* **1966**, *14*, 491–497. [CrossRef]
30. Panguluri, R.P.; Zeng, C.; Weitering, H.H.; Sullivan, J.M.; Erwin, S.C.; Nadgorny, B. Spin Polarization and Electronic Structure of Ferromagnetic Mn_5Ge_3 Epilayers. *Phys. Status Solidi B* **2005**, *242*, R67–R69. [CrossRef]
31. Olive-Mendez, S.; Spiesser, A.; Michez, L.A.; Le Thanh, V.; Glachant, A.; Derrien, J.; Devillers, T.; Barski, A.; Jamet, M. Epitaxial Growth of Mn_5Ge_3/Ge(111) Heterostructures for Spin Injection. *Thin Solid Film.* **2008**, *517*, 191–196. [CrossRef]
32. Ndiaye, W.; Richter, M.C.; Heckmann, O.; De Padova, P.; Mariot, J.-M.; Stroppa, A.; Picozzi, S.; Wang, W.; Taleb-Ibrahimi, A.; Le Fèvre, P.; et al. Bulk Electronic Structure of Mn_5Ge_3/Ge(111) Films by Angle-Resolved Photoemission Spectroscopy. *Phys. Rev. B* **2013**, *87*, 165137. [CrossRef]
33. Tang, J.; Wang, C.-Y.; Chang, L.-T.; Fan, Y.; Nie, T.; Chan, M.; Jiang, W.; Chen, Y.-T.; Yang, H.-J.; Tuan, H.-Y.; et al. Electrical Spin Injection and Detection in Mn_5Ge_3/Ge/Mn_5Ge_3 Nanowire Transistors. *Nano Lett.* **2013**, *13*, 4036–4043. [CrossRef] [PubMed]
34. Spiesser, A.; Saito, H.; Jansen, R.; Yuasa, S.; Ando, K. Large Spin Accumulation Voltages in Epitaxial Mn_5Ge_3 Contacts on Ge without an Oxide Tunnel Barrier. *Phys. Rev. B* **2014**, *90*, 205213. [CrossRef]
35. Xie, Y.; Yuan, Y.; Birowska, M.; Zhang, C.; Cao, L.; Wang, M.; Grenzer, J.; Kriegner, D.; Doležal, P.; Zeng, Y.-J.; et al. Strain-Induced Switching between Noncollinear and Collinear Spin Configuration in Magnetic Mn_5Ge_3 Films. *Phys. Rev. B* **2021**, *104*, 064416. [CrossRef]
36. Toliński, T.; Synoradzki, K. Specific Heat and Magnetocaloric Effect of the Mn_5Ge_3 Ferromagnet. *Intermetallics* **2014**, *47*, 1–5. [CrossRef]
37. Zheng, T.F.; Shi, Y.G.; Hu, C.C.; Fan, J.Y.; Shi, D.N.; Tang, S.L.; Du, Y.W. Magnetocaloric Effect and Transition Order of Mn_5Ge_3 Ribbons. *J. Magn. Magn. Mater.* **2012**, *324*, 4102–4105. [CrossRef]
38. Lalita; Rathi, A.; Pardeep; Verma, A.K.; Gahtori, B.; Gautam, A.; Pant, R.P.; Babu, P.D.; Basheed, G.A. Field Dependence of Magnetic Entropy Change in Mn_5Ge_3 near Room Temperature. *J. Alloy. Compd.* **2021**, *876*, 159908. [CrossRef]
39. Maraytta, N.; Voigt, J.; Salazar Mejía, C.; Friese, K.; Skourski, Y.; Perßon, J.; Salman, S.M.; Brückel, T. Anisotropy of the Magnetocaloric Effect: Example of Mn_5Ge_3. *J. Appl. Phys.* **2020**, *128*, 103903. [CrossRef]
40. Wang, S.; Fan, C.; Liu, D. Large Anisotropic Magnetocaloric Effect, Wide Operating Temperature Range, and Large Refrigeration Capacity in Single-Crystal Mn_5Ge_3 and Mn_5Ge_3/$Mn_{3.5}Fe_{1.5}Ge_3$ Heterostructures. *ACS Appl. Mater. Interfaces* **2021**, *13*, 33237–33243. [CrossRef]
41. Kim, Y.; Kim, E.J.; Choi, K.; Han, W.B.; Kim, H.-S.; Yoon, C.S. Magnetocaloric Effect of $Mn_{5+x}Ge_{3-x}$ Alloys. *J. Alloy. Compd.* **2015**, *620*, 164–167. [CrossRef]
42. Kim, Y.; Kang, K.H.; Kim, J.H.; Kim, E.J.; Choi, K.; Han, W.B.; Kim, H.-S.; Oh, Y.; Yoon, C.S. Magnetocaloric Refrigerant with Wide Operating Temperature Range Based on $Mn_{5-x}Ge_3(Co,Fe)_x$ Composite. *J. Alloy. Compd.* **2015**, *644*, 464–469. [CrossRef]

43. Carroll, P.; Williams, A.; Caudle, M.; Darkins, L.; Eaton, A.; Fitzgerald, B.; Knauf, B.; Rurka, M.; Shlonsky, E.; Wilson, P.; et al. Enhanced Magnetic Refrigeration Capacities in Minutely Co Doped $Mn_{5-x}Co_xGe_3$ Compounds. *Intermetallics* **2017**, *89*, 10–15. [CrossRef]
44. Kang, K.H.; Kim, J.H.; Oh, Y.; Kim, E.J.; Yoon, C.S. Critical Behavior and Magnetocaloric Effect of $Mn_{4.75}Ge_3(Co, Fe)_{0.25}$ Alloys. *J. Alloy. Compd.* **2017**, *696*, 931–937. [CrossRef]
45. Kang, K.H.; Kim, J.H.; Kim, J.W.; Chung, K.C.; Yoon, C.S. Direct Measurement of the Magnetocaloric Effect (ΔT_{ad}) of $Mn_{5-x}(Fe,Co)_xGe_3$. *J. Alloy. Compd.* **2017**, *729*, 603–606. [CrossRef]
46. Zhang, Q.; Du, J.; Li, Y.B.; Sun, N.K.; Cui, W.B.; Li, D.; Zhang, Z.D. Magnetic Properties and Enhanced Magnetic Refrigeration in $(Mn_{1-x}Fe_x)_5Ge_3$ Compounds. *J. Appl. Phys.* **2007**, *101*, 123911. [CrossRef]
47. Brock, J.; Bell-Pactat, N.; Cai, H.; Dennison, T.; Fox, T.; Free, B.; Mahyub, R.; Nar, A.; Saaranen, M.; Schaeffer, T.; et al. The Effect of Fe Doping on the Magnetic and Magnetocaloric Properties of $Mn_{5-x}Fe_xGe_3$. *Adv. Mater. Sci. Eng.* **2017**, *2017*, 9854184. [CrossRef]
48. Kang, K.H.; Kim, E.J.; Kim, J.; Yoon, C.S. $Mn_{5-x}Ge_3Ni_x$ Refrigerant for Active Magnetic Refrigeration. *J. Appl. Phys.* **2020**, *128*, 223903. [CrossRef]
49. Liu, X.B.; Altounian, Z. Magnetocaloric Effect in $Mn_5Ge_{3-x}Si_x$ Pseudobinary Compounds. *J. Appl. Phys.* **2006**, *99*, 08Q101. [CrossRef]
50. Zhao, F.Q.; Dagula, W.; Tegus, O.; Buschow, K.H.J. Magnetic-Entropy Change in $Mn_5Ge_{3-x}Si_x$ Alloys. *J. Alloy. Compd.* **2006**, *416*, 43–45. [CrossRef]
51. Xi-Bin, L.; Shao-Ying, Z.; Bao-Gen, S. Magnetic Properties and Magnetocaloric Effects of $Mn_5Ge_{3x}Ga_x$. *Chin. Phys.* **2004**, *13*, 397–400. [CrossRef]
52. Songlin; Dagula; Tegus, O.; Brück, E.; de Boer, F.R.; Buschow, K.H.J. Magnetic and Magnetocaloric Properties of $Mn_5Ge_{3-x}Sb_x$. *J. Alloy. Compd.* **2002**, *337*, 269–271. [CrossRef]
53. Zheng, T.F.; Shi, Y.G.; Fan, J.Y.; Shi, D.N.; Tang, S.L.; Lv, L.Y.; Zhong, W. Critical Behavior and the Universal Curve for Magnetocaloric Effect in Textured $Mn_5Ge_{3-x}Al_x$ Ribbons. *J. Appl. Phys.* **2013**, *113*, 17A944. [CrossRef]
54. Si, X.; Liu, Y.; Zhang, Z.; Ma, X.; Lin, J.; Luo, X.; Zhong, Y.; Si, H. Analysis of the Magnetic Transition and Magnetocaloric Effect in $Mn_5Ge_{2.9}Ag_{0.1}$ Compound. *J. Alloy. Compd.* **2019**, *795*, 304–313. [CrossRef]
55. Qian, Y.; Ma, X.; Si, X.; Liu, H.; Luo, X.; Lin, J.; Liu, Y. The Analysis of Magnetocaloric Effect and Magnetic Critical Behavior in $Mn_5Ge_{3-x}Ag_x$ Compounds. *Phys. Scr.* **2020**, *95*, 065701. [CrossRef]
56. Swathi, S.; Arun, K.; Remya, U.D.; Dzubinska, A.; Reiffers, M.; Nagalakshmi, R. Ising Critical Behavior and Room Temperature Magnetocaloric Effect in Itinerant Ferromagnetic $Mn_5Ge_{2.9}Fe_{0.1}$ Compound. *Intermetallics* **2021**, *132*, 107164. [CrossRef]
57. Halder, M.; Yusuf, S.M.; Nigam, A.K. Magnetocaloric Effect and Its Implementation in Critical Behavior Study of $Mn_4FeGe_{3-x}Si_x$ Intermetallic Compounds. *J. Appl. Phys.* **2011**, *110*, 113915. [CrossRef]
58. Sun, Y.W.; Yan, J.L.; Feng, E.L.; Tang, G.W.; Zhou, K.W. Effect of Fe Substitution on the Structure and Magnetocaloric Effect of $Mn_{5-x}Fe_xGeSi_2$ Alloys. *J. Magn. Magn. Mater.* **2017**, *422*, 356–361. [CrossRef]
59. Rodríguez-Carvajal, J. Recent Advances in Magnetic Structure Determination by Neutron Powder Diffraction. *Phys. B Condens. Matter* **1993**, *192*, 55–69. [CrossRef]
60. Forsyth, J.B.; Brown, P.J. The Spatial Distribution of Magnetisation Density in Mn_5Ge_3. *J. Phys. Condens. Matter* **1990**, *2*, 2713–2720. [CrossRef]
61. Synoradzki, K.; Kowalski, W.; Falkowski, M.; Toliński, T.; Kowalczyk, A. Magnetic Properties and Magnetocaloric Effect of $DyNi_4Si$. *Acta Phys. Pol. A* **2014**, *126*, 162–163. [CrossRef]
62. Zhang, F.; Taake, C.; Huang, B.; You, X.; Ojiyed, H.; Shen, Q.; Dugulan, I.; Caron, L.; van Dijk, N.; Brück, E. Magnetocaloric Effect in the $(Mn,Fe)_2(P,Si)$ System: From Bulk to Nano. *Acta Mater.* **2022**, *224*, 117532. [CrossRef]
63. Langford, J.I.; Wilson, A.J.C. Scherrer after Sixty Years: A Survey and Some New Results in the Determination of Crystallite Size. *J. Appl. Crystallogr.* **1978**, *11*, 102–113. [CrossRef]
64. Gschneidner, K.A., Jr.; Pecharsky, V.K.; Tsokol, A.O. Recent Developments in Magnetocaloric Materials. *Rep. Prog. Phys.* **2005**, *68*, 1479–1539. [CrossRef]
65. Toliński, T.; Falkowski, M.; Kowalczyk, A.; Synoradzki, K. Magnetocaloric Effect in the Ternary $DyCo_3B_2$ Compound. *Solid State Sci.* **2011**, *13*, 1865–1868. [CrossRef]
66. Coey, J.M.D. *Magnetism and Magnetic Materials*; Cambridge University Press: Cambridge, UK, 2010; ISBN 978-0-521-81614-4.
67. Ciszewski, R. Magnetic Structure of the Mn_5Ge_3 Alloy. *Phys. Status Solidi (B)* **1963**, *3*, 1999–2004. [CrossRef]
68. Synoradzki, K.; Toliński, T. Effective Mass Enhancement and Spin-Glass Behaviour in $CeCu_4Mn_yAl_{1-y}$ Compounds. *J. Phys. Condens. Matter* **2012**, *24*, 136003. [CrossRef] [PubMed]
69. Synoradzki, K. Spin-Glass Behavior in $LaCu_4Mn$ Compound. *Acta Phys. Pol. A* **2017**, *131*, 1024–1026. [CrossRef]
70. Synoradzki, K. Magnetocaloric Effect in Spin-Glass-like $GdCu_4Mn$ Compound. *J. Magn. Magn. Mater.* **2022**, *546*, 168857. [CrossRef]
71. Kang, K.H.; Oh, Y.; Kim, J.H.; Kim, E.J.; Kim, H.-S.; Yoon, C.S. Magnetocaloric Effect of Compositionally Partitioned $Mn_{5-x}Ge_3Ni_x$ Alloys Produced by Solid State Sintering. *J. Alloy. Compd.* **2016**, *681*, 541–546. [CrossRef]
72. Kappel, G.; Fischer, G.; Jaegle, A. On the Saturation Magnetization of Mn_5Ge_3. *Phys. Lett. A* **1973**, *45*, 267–268. [CrossRef]
73. Arrott, A. Criterion for Ferromagnetism from Observations of Magnetic Isotherms. *Phys. Rev.* **1957**, *108*, 1394–1396. [CrossRef]
74. Pecharsky, V.K.; Gschneidner, K.A. Magnetocaloric Effect from Indirect Measurements: Magnetization and Heat Capacity. *J. Appl. Phys.* **1999**, *86*, 565–575. [CrossRef]

75. Griffith, L.D.; Mudryk, Y.; Slaughter, J.; Pecharsky, V.K. Material-Based Figure of Merit for Caloric Materials. *J. Appl. Phys.* **2018**, *123*, 034902. [CrossRef]
76. Franco, V.; Blázquez, J.S.; Conde, A. Field Dependence of the Magnetocaloric Effect in Materials with a Second Order Phase Transition: A Master Curve for the Magnetic Entropy Change. *Appl. Phys. Lett.* **2006**, *89*, 222512. [CrossRef]
77. Le Guillou, J.C.; Zinn-Justin, J. Critical Exponents from Field Theory. *Phys. Rev. B* **1980**, *21*, 3976–3998. [CrossRef]
78. Zverev, V.I.; Tishin, A.M.; Kuz'min, M.D. The Maximum Possible Magnetocaloric ΔT Effect. *J. Appl. Phys.* **2010**, *107*, 043907. [CrossRef]
79. Law, J.Y.; Franco, V. Magnetocaloric Composite Materials. In *Encyclopedia of Materials: Composites*; Elsevier: Amsterdam, The Netherlands, 2021; pp. 461–472, ISBN 978-0-12-819731-8.
80. de Oliveira, R.C.; Demaille, D.; Casaretto, N.; Zheng, Y.J.; Marangolo, M.; Mosca, D.H.; Varalda, J. Magnetic and Structural Properties of $Mn_{5+x}Ge_{3+y}$ Thin Films as a Function of Substrate Orientation. *J. Magn. Magn. Mater.* **2021**, *539*, 168325. [CrossRef]